

Slowdown of light due to exciton-polariton propagation in ZnO

Shula Chen, Weimin Chen and Irina Boyanova

Linköping University Post Print

N.B.: When citing this work, cite the original article.

Original Publication:

Shula Chen, Weimin Chen and Irina Boyanova, Slowdown of light due to exciton-polariton propagation in ZnO, 2011, Physical Review B. Condensed Matter and Materials Physics, (83), 24, 245212.

<http://dx.doi.org/10.1103/PhysRevB.83.245212>

Copyright: American Physical Society

<http://www.aps.org/>

Postprint available at: Linköping University Electronic Press

<http://urn.kb.se/resolve?urn=urn:nbn:se:liu:diva-69847>

Slowdown of light due to exciton-polariton propagation in ZnO

S. L. Chen, W. M. Chen, and I. A. Buyanova*

Department of Physics, Chemistry and Biology, Linköping University, 58183 Linköping, Sweden

(Received 1 February 2011; revised manuscript received 15 April 2011; published 30 June 2011)

By employing time-of-flight spectroscopy, the group velocity of light propagating through bulk ZnO is demonstrated to dramatically decrease down to 2044 km/s when photon energy approaches the absorption edge of the material. The magnitude of this decrease is found to depend on light polarization. It is concluded that even though the slowdown is observed in the vicinity of donor bound exciton (BX) resonances, the effect is chiefly governed by dispersion of free exciton (FX) polaritons that propagate coherently via ballistic transport. Based on the experimentally determined spectral dependence of the polariton group velocity, the polariton dispersion is accurately determined.

DOI: [10.1103/PhysRevB.83.245212](https://doi.org/10.1103/PhysRevB.83.245212)

PACS number(s): 78.66.Hf, 78.47.D–

I. INTRODUCTION

There has been substantial fundamental and technological interest^{1–5} to control and slow down light propagation in dispersive materials attributable to its great potential for a variety of innovative applications, e.g., in all optical communication networks, novel acousto-optical devices, quantum information storage and processing, etc. For example, it was shown⁶ that slowing the group velocity of a laser pulse down to the speed of sound in solids leads to enhanced acousto-optical effects, which is promising for applications in quantum optics for effective wave mixing and amplification. Implementation of controllable slow-light delays^{7,8} in photonic-crystal waveguides and fibers enables realization of all-optical buffers and variable optical delays. Moreover, laser pulses have even been brought to a halt in opaque atomic medium, which allowed storage of coherent optical information for up to 1 ms.^{9,10} This represents an important step toward quantum information storage and processing. In semiconductor materials the concept of slow light can be realized by utilizing singularities of dielectric function in the vicinity of excitonic resonances and exciton-photon coupling that leads to polariton formation. By using time-of-flight spectroscopy, a decrease in light group velocity owing to polariton dispersion has indeed been experimentally demonstrated for a variety of bulk semiconductors and related low-dimensional structures including bulk CdSe,¹¹ GaP,¹² CuCl,¹³ GaN,¹⁴ CdZnTe,¹⁵ and GaAs quantum wells.¹⁶

In recent years ZnO has been recognized to be among the most promising semiconductor materials for optical and electronic applications. As a wide bandgap semiconductor with a direct bandgap and large exciton-binding energy of about 60 meV, ZnO is a key candidate not only for biodetection and transparent electronics but also in optical communications, high-density data storage systems, as well as for short wavelength light emitters including lasers. Moreover light-matter interaction effects, such as polariton formation, are known^{17–19} to be exceptionally strong in ZnO, facilitated by the polar-bonding character and large polarizability of ZnO matrix. Therefore polaritonic effects are foreseen to contribute to novel fascinating applications of this material, e.g., in polariton lasers operating at room temperature.²⁰

In principle the polariton formation should also substantially affect group velocity of light propagating through ZnO

media. The first experimental verification that the light can indeed be slowed down in ZnO was recently obtained from time-resolved photoluminescence (PL) studies of donor bound exciton (BX) emission.²¹ It was found that time required for transfer of the emitted photons from the BX recombination through a 1-mm ZnO crystal is rather long, i.e., reaching 200 ps, which was attributed to the dispersive propagation of the BX polaritons. However, analysis of the results was complicated by the fact that the delay of the detected BX emission was partly related to delayed formation of the BX following expansion of electron-hole plasma through the crystal from the front surface of the sample where it was initially excited.

In the present study we avoid this complication by investigating propagation of *laser pulses* instead. We show that light experiences dramatic slowdown when photon energies approach the absorption edge of ZnO, to a degree determined by light polarization. This effect is analyzed in the framework of polariton propagation. It is concluded that even though the slowdown is observed in the vicinity of donor BX resonances, the main contribution to the effect in fact arises from free exciton (FX) polaritons that propagate coherently via ballistic transport. Based on the experimentally determined spectral dependence of the polariton group velocity, the polariton dispersion is accurately determined.

II. SAMPLES AND METHODS

Light propagation was studied by time-of-flight spectroscopy using commercially available c-plane ZnO substrates from Cermet, Inc. and Denpa Co. with thicknesses of 0.25 and 0.55 mm, respectively. To reduce light absorption in the vicinity of excitonic resonances, some of the Denpa ZnO substrates were mechanically polished down to the thickness of 0.13 mm. Effects of polarization of light on its group velocity in the wurtzite matrix were evaluated by performing time-of-flight measurements for the following relative orientations of the light wave vector \mathbf{k} , the electrical field vector \mathbf{E} , and the principal axis \mathbf{c} of wurtzite ZnO: (i) $\mathbf{k} \parallel \mathbf{c}$, $\mathbf{E} \perp \mathbf{c}$ (α -polarization); (ii) $\mathbf{k} \perp \mathbf{c}$, $\mathbf{E} \perp \mathbf{c}$ (σ -polarization); and (iii) $\mathbf{k} \perp \mathbf{c}$, $\mathbf{E} \parallel \mathbf{c}$ (π -polarization). In the two latter cases, a 1-mm-thick sample cut from the Denpa ZnO substrate was used.

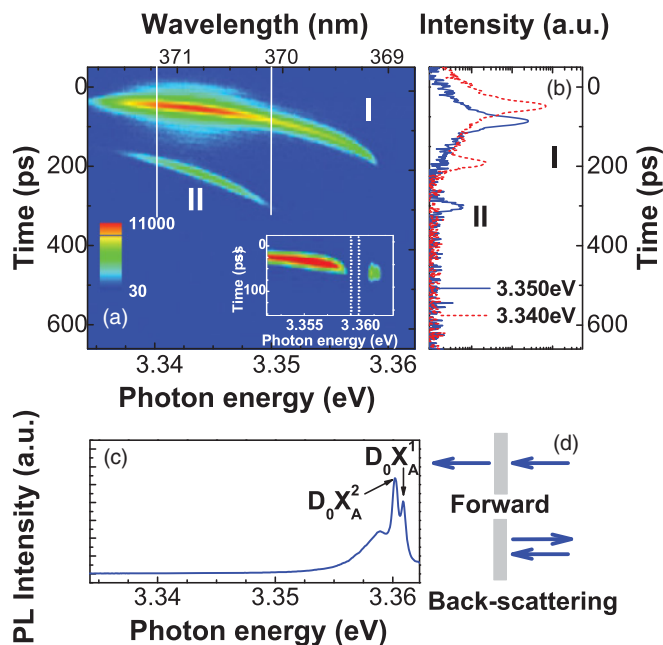


FIG. 1. (Color online) (a) Transient spectra of a 3.351-eV laser pulse transmitted through the 0.55-mm ZnO sample in the α -measurement geometry ($k \parallel c$, $E \perp c$). The light intensity is displayed in the logarithmic scale. The stronger signal denoted as “I” corresponds to the main laser pulse, whereas the weaker component “II” is attributed to the light pulse that has experienced two internal reflections at the sample surfaces before exiting the sample. (b) Temporal profiles of the transmitted light with energies as indicated by the solid lines in (a). (c) Typical PL spectrum recorded in the back-scattering geometry. All measurements were performed at 4 K. (d) A schematic illustration of the measurement geometries employed in the time-of-flight and PL measurements. The inset in (a) shows a close up of the transient spectra within the D_0X_A spectral region. The dotted lines in the inset indicate the spectral positions of the $D_0X_A^1$ and $D_0X_A^2$ resonances. The spectra were measured for the 0.13-mm-thick ZnO.

Time-resolved optical measurements were carried out at temperatures of 4–150 K using a tunable Ti:sapphire femtosecond-pulsed laser with a repetition frequency of 76 MHz and duration of about 150 fs. Second-harmonic laser pulses tuned below the FX but in the vicinity of BX energies (3.326–3.361 eV) were used as a light source during time-of-flight measurements. This allowed us to solely study propagation of the laser light and to avoid PL excitation. The transmitted light was detected in the forward geometry with light propagating along the normal to the sample surface [Fig. 1(d)]. The time origin was calibrated by carefully removing the sample out of the beam. Typical laser power was around 10 W/cm². PL measurements were performed in the back-scattering geometry under excitation by third-harmonic laser pulses with the photon energy of 4.66 eV. The transmitted laser light and PL were detected by a Hamamatsu streak camera combined with a 0.5-m grating monochromator. Time resolution of the whole system was better than 2 ps.

III. EXPERIMENTAL RESULTS

Figure 1(a) shows a representative image of a laser pulse, which was initially tuned to 3.351 eV, after it was

transmitted through a 0.55-mm-thick Cermet ZnO sample in the α -measurement geometry ($k \parallel c$, $E \perp c$). Several important features can be noticed. First of all, the light could only be transmitted when photon energies are below 3.360 eV, which indicates strong near-band-edge absorption at the higher energies. [After decreasing thickness of the sample down to 0.13 mm, light propagation can be studied even for photon energies slightly above the D^0X_A resonances as shown in the inset of Fig. 1(a)]. Second, the image (i.e., streak) of the transmitted light is strongly bent toward the absorption edge. This means that the time required for light propagation through the sample (to be referred further as time delay) critically depends on photon energy and increases when the photon energy approaches the region of near-band-edge excitonic absorption. For example the time delay for the main component (denoted as “I”) increases from about 49 ps for the 3.335 eV photons to up to 217 ps for the 3.360 eV photons. This dependence can also be seen from Fig. 1(b), which shows time profiles of the transmitted light for energies as indicated by the solid lines in Fig. 1(a). Moreover, in addition to the intense signal from the main laser pulse, the image contains a much weaker signal denoted as “II” in Figs. 1(a) and 1(b). The corresponding time delay at any wavelength is about three times longer than that for the main transmitted pulse, which results in stronger bending of the streak. We attribute this feature to the light pulse which has experienced two internal reflections at the sample surfaces (which act as a Fabry-Perot cavity) before exiting the sample, i.e., propagated inside the sample in forward-backward-forward directions. Comparison with the reference PL spectra [Fig. 1(c)] shows that the observed slowdown occurs in the vicinity of donor BX resonances denoted as $D^0X_A^1$ and $D^0X_A^2$ in Fig. 1(c).

The slowdown of photons with energies in the vicinity of the absorption edge is also observed in the π - (i.e., when $k \perp c$, $E \parallel c$) and σ - (i.e., when $k \perp c$, $E \perp c$) geometries, as shown in Figs. 2(a) and 2(b), respectively. In these cases, however, only the main transmitted pulse is observed, likely due to poorer quality of the surfaces after cutting the sample. In the σ -geometry light propagation remains basically identical to that observed in the α -geometry discussed previously. On the other hand it is significantly modified when the light wave has π -polarization. Under this condition the ZnO samples become transparent in the regions of the $D^0X_A^1$ and $D^0X_A^2$ absorption, and a blue shift of the absorption edge up to approximately 3.375 eV is observed. With increasing power of the laser light up to 800 W/cm², the transmitted signal can be detected within the spectral range of 3.3771–3.3810 eV (i.e., above the 3.375-eV resonance) even for the 1-mm-thick ZnO [see the inset of Fig. 2(a)]. It is also noticeable that the bending of the streak toward the absorption edge is by far less pronounced for the π -polarization, meaning shorter time delays.

The observed dependence of the light absorption on light polarization can be understood in light of selection rules for optical transitions in the wurtzite matrix. Indeed, crystal-field and spin-orbit interactions split valence band (VB) of ZnO into the so-called A-, B-, and C-subbands. Assuming an inverse ordering of the VB states,^{22–24} i.e., A(Γ_7), B(Γ_9), and C(Γ_7) states, symmetries of the corresponding excitonic states in ZnO are $\Gamma_7 \otimes \Gamma_7 = \Gamma_1 \otimes \Gamma_2 \otimes \Gamma_5$, $\Gamma_7 \otimes \Gamma_9 = \Gamma_6 \otimes \Gamma_5$,

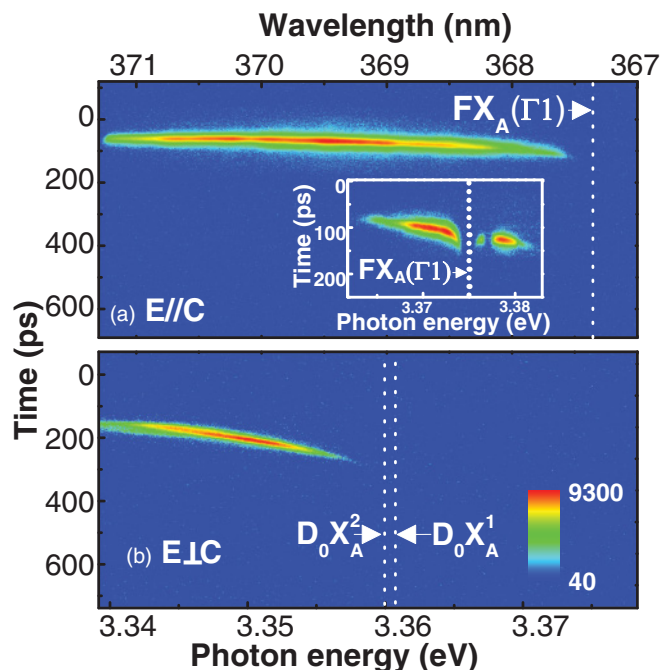


FIG. 2. (Color online) Transient spectra of a 3.358-eV laser pulse with the (a) π - and (b) σ -polarization after transmission through the 1-mm-thick ZnO sample. The light intensity is displayed in the logarithmic scale. The dotted lines indicate positions of the specified excitonic resonances. The employed laser power was around 10 W/cm^2 . The inset in (a) shows a close up of the transient spectra in the vicinity of the 3.375-eV resonance. The spectra were measured after increasing the laser power to 800 W/cm^2 .

and $\Gamma_7 \otimes \Gamma_7 = \Gamma_1 \otimes \Gamma_2 \otimes \Gamma_5$ for the A-, B-, and C-excitons, respectively. From group theory considerations the only dipole-allowed transitions are Γ_5 for $E \perp c$ and Γ_1 for $E \parallel c$ polarizations. Moreover, oscillator strengths of the A and B Γ_5 excitons are significantly larger than that for the C Γ_5 . On the other hand the A Γ_1 excitons are spin-forbidden and consequently have low oscillator strength, whereas the C Γ_1 excitons are spin-allowed.²⁴ Therefore, optical-absorption transitions related to the upper A- and B-VB subbands (and the associated D^0X resonances) are the most pronounced ones in the α - and σ -geometries, consistent with our experimental data. In contrast the A Γ_1 resonance, which defines the ZnO absorption edge for the $E \parallel c$ light polarizations, is rather weak. Spectral positions of the relevant excitonic resonances are indicated by the dotted lines in Figs. 2 and 3. From the inset in Fig. 2(a) one may also notice the presence of an even weaker resonance located at $\sim 2 \text{ meV}$ above the A Γ_1 . The spectral position of this resonance corresponds to that of a longitudinal A Γ_{5L} exciton,²³ which may become weakly visible when $E \parallel c$ because of, e.g., coupling with A Γ_1 or imperfect optical alignment. This resonance will, however, not be further considered as it has a very low oscillator strength and does not affect time delays of the transmitted light.

The results from the time-of-flight measurements of all investigated samples obtained in three measurement geometries are summarized in Fig. 3, where symbols denote the experimentally measured delay times for the ZnO samples with the specified thicknesses. Data denoted by dots represent

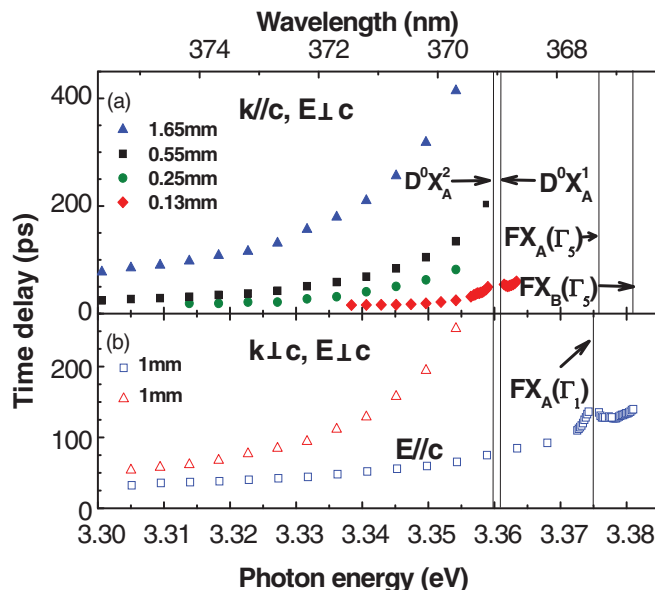


FIG. 3. (Color online) Time delays of laser pulses caused by propagation through the ZnO media with the specified thickness for (a) $k \parallel c$ and (b) $k \perp c$. The data points attributed to the 1.65-mm-thick ZnO represent time delays for the signal “II” shown in Fig. 1, i.e., for a laser pulse that has undergone the forward-backward-forward propagation inside the 0.55-mm sample. The solid lines represent spectral positions of the marked excitonic resonances.

the time delays in the Cermet ZnO, whereas all other data were obtained from the Denpa samples. Clearly the slowdown effect is common in ZnO and relies on the presence of excitonic resonances as a magnitude of the effect largely depends on light polarization.

Light propagation also remains dispersive at elevated temperatures. This is illustrated in Fig. 4 where spectral dependences of the delay time measured at different temperatures in

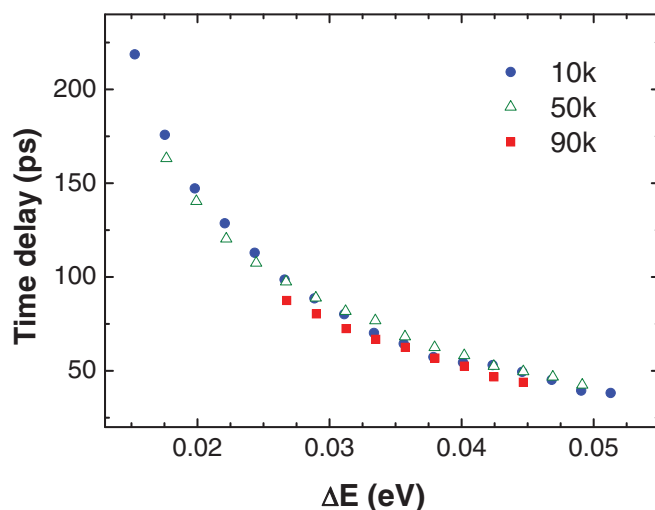


FIG. 4. (Color online) Time delays of the transmitted laser pulse measured from the 0.55-mm-thick ZnO at the specified temperatures. The data are plotted as a function of energy distance ΔE to the $FX_A(\Gamma_5)$ exciton to account for a temperature-induced shift of the ZnO bandgap.

the α -geometry are shown. The data are plotted as a function of energy distance to the $\text{FX}_A(\Gamma_5)$ exciton to account for a temperature-induced shift of the ZnO bandgap and, therefore, of the spectral position of the $\text{FX}_A(\Gamma_5)$. The latter was determined based on the performed temperature-dependent PL studies. The measurements were unfortunately limited to temperatures up to 90 K, as strong broadening of the absorption edge at higher temperatures hampered light transmission close to the excitonic resonances.

IV. DISCUSSION

A. Mechanism for light propagation

Before discussing the origin of the observed slowdown of light in ZnO in the vicinity of the excitonic resonances, let us first elucidate the mechanism responsible for light propagation. In a dielectric medium, light propagation could be either ballistic^{11,12,14} or diffusive¹⁴ depending on concentration and scattering cross-section of scattering centers in the material. Both mechanisms could, in principle, account for the resonant decrease of light velocity in the regions of excitonic resonances.¹⁴ However while the diffusive propagation features a broad outgoing angle of the transmitted light, a narrow angular distribution is expected in the ballistic regime. This allows us to discriminate between these mechanisms by measuring the angular distribution of light intensity after transmission through the sample. Representative results are shown in Figs. 5(a) and 5(b) for the Denpa and Cermet ZnO, respectively. Only a very weak divergence of the transmitted laser light, which is independent of the photon energy, is observed suggesting that the light propagation in the investigated samples is predominantly ballistic. This conclusion is further supported by the observation of the “reflection” streak [signal “II” in Figs. 1(a) and 1(b)], i.e., the transmitted laser pulse that experienced two internal reflections. This finding indicates weak scattering of the laser light, which is characteristic for the ballistic regime. We note, however, that the “reflection” signal was not detected in the Cermet ZnO, which may imply a weak contribution of the diffusive component.

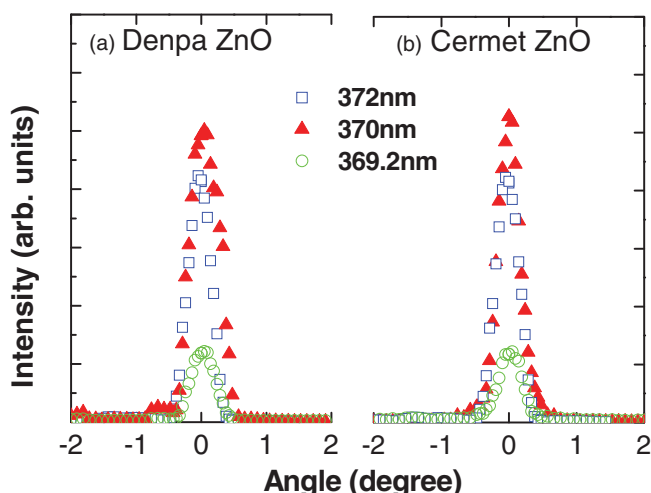


FIG. 5. (Color online) Angular distributions of the transmitted light, with the wavelengths of 369.2, 370 and 372 nm, through the (a) Denpa and (b) Cermet ZnO.

Under conditions of the ballistic transport, light wave will propagate coherently with a group velocity v_g defined as

$$v_g(E) = \frac{1}{\hbar} \frac{dE}{dK}. \quad (1)$$

Since the time required for light propagation in this regime linearly depends on the sample thickness L , the group velocity and its dispersion can be experimentally determined by $v_g = L/T_d$ from the measured time delay T_d . The obtained spectral dependence of v_g is shown in Fig. 6. It provides evidence that the light velocity in ZnO dramatically decreases down to $\sim 2 \times 10^6$ m/s, i.e., 1500 times slower than the speed of light in vacuum, when approaching excitonic resonances. Moreover, under these conditions the group velocity can be controlled by changing polarization of the propagating light, e.g., from 2×10^6 m/s when $\mathbf{E} \perp \mathbf{c}$ to 1.1×10^7 m/s when $\mathbf{E} \parallel \mathbf{c}$ for the 3.365-eV photons.

B. Origin of the slowdown effect

The observed spectral dependence of the group velocity can be understood by taking into account exciton-photon coupling, which leads to the formation of a mixed-mode state called exciton-polariton that is now a true eigenstate of the system. Within the polariton framework the light wave entering the sample is converted into the polariton wave which then propagates through the media with the group velocity determined by the polariton dispersion.^{14,17,18} In the case of several excitonic resonances the dispersion of the exciton-polaritons neglecting the spatial dispersion can be expressed as

$$\frac{\hbar^2 c^2 K^2}{E^2} = \varepsilon_\infty + \sum_{i=D^0X_A^i} \frac{f_i E_{0i}^2}{E_{0i}^2 - E^2 - iE\hbar\Gamma_i} + \sum_{j=A,B,C} \frac{f_j E_{0j}^2}{E_{0j}^2 - E^2 - iE\hbar\Gamma_j}. \quad (2)$$

Here ε_∞ is the background dielectric constant. The second and the third term represent contributions from the D^0X and FX resonances, respectively, where the summation should be done over all optically active states. E_0 , f , and Γ are the resonance energy, oscillator strength, and the damping constant (considered to be wavevector \mathbf{K} independent), respectively. The subscript i (j) denotes the association of these parameters to the specific D^0X (FX) resonance. We would like to note that even though the polariton concept in ZnO has usually been applied to FX polaritons, contributions of the BXs were also included in Eq. (2) for completeness of the analysis.¹⁴ Equations (1) and (2) can be used to simulate spectral dependence of the polariton-group velocity. The corresponding results are shown by the solid (black dashed) lines in Fig. 6 for the Denpa (Cermet) ZnO using the parameters given in Table I. The background dielectric constants ε_∞ for $\mathbf{E} \perp \mathbf{c}$ and $\mathbf{E} \parallel \mathbf{c}$ light polarizations were set to 6.69 and 7.47, respectively.²⁵ The damping term $\hbar\Gamma_j$ for all resonances was assumed to be 0.5 meV, which is of the order of the PL linewidth. For the Denpa ZnO only $D^0X_A^1$ and $D^0X_A^2$ resonances were considered, and the ratio between their oscillator strengths was estimated based on the measured ratio between the

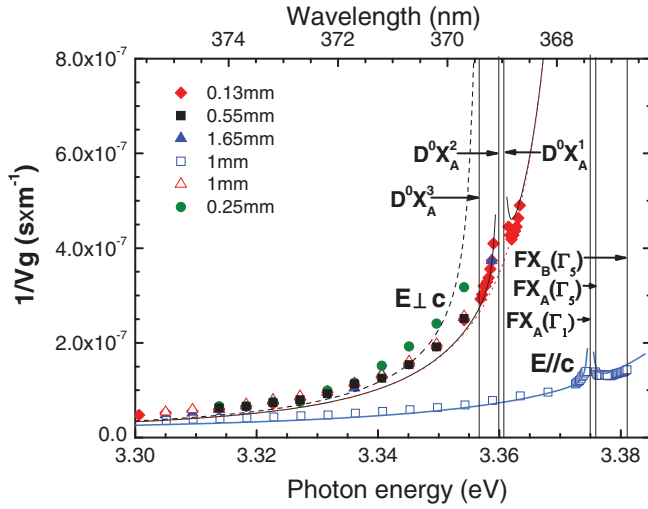


FIG. 6. (Color online) Spectral dependence of the reverse group velocity. The symbols represent experimental data, and the curves are the simulation results using Eq. (2) with the parameters listed in Table I. The solid (dashed) curves represent a best fit for the Denpa (Cermet) ZnO. The red dotted curve represents results of the simulations performed by omitting contributions of all D^0X resonances. Note that the simulated time delays within the spectral range of the strong absorption from the D^0X and $FX_A(\Gamma_1)$ resonances are not shown here for clarity. The vertical lines denote the spectral positions of the excitonic resonances as specified.

corresponding PL intensities. For the Cermet sample, another resonance at 3.3567 eV ($D^0X_A^3$) observed in both transmission and PL spectra was also included. The spectral positions of the FX resonances were taken from Refs. 17 and 26, while their f_j values were chosen based on the reported values¹⁷ of the corresponding longitudinal-transverse splitting. These values are consistent with the measured spectral positions of the D^0X_A and FX-PL lines in the investigated samples, which are in excellent agreement with the reported values for bulk strain-free ZnO.²⁶ The oscillator strengths for the D^0X resonances were treated as fitting parameters. The best fit to the experimental data for the $\mathbf{E} \perp \mathbf{c}$ light polarizations was obtained assuming $f(D^0X_A^1) = 1.3 \times 10^{-5}$ and $f(D^0X_A^2) = 2.6 \times 10^{-5}$ for the Denpa ZnO (shown by the black solid line in Fig. 6), whereas higher oscillator strengths for these

TABLE I. The parameters of the excitonic resonances obtained from a best fit of Eqs. (1) and (2) to the experimental data.

Transition	E_0 (eV)	Oscillator strength, f	
		$\mathbf{E} \perp \mathbf{c}$	$\mathbf{E} \parallel \mathbf{c}$
$FX_A(\Gamma_5)$	3.3758	0.0071	0
$FX_B(\Gamma_5)$	3.3810	0.0404	0
$FX_A(\Gamma_1)$	3.3750	0	0.0009
$FX_C(\Gamma_1)$	3.4198	0	0.0727
$D_0X_A^1$ (Denpa)	3.3608	1.3×10^{-5}	0
$D_0X_A^1$ (Cermet)	3.3608	8.8×10^{-4}	0
$D_0X_A^2$ (Denpa)	3.3600	2.6×10^{-5}	0
$D_0X_A^2$ (Cermet)	3.3600	8.8×10^{-4}	0
$D_0X_A^3$ (Cermet)	3.3567	1.7×10^{-3}	0

resonances (see Table I) were required to reproduce the $v_g(E)$ dependence for the Cermet sample (shown by the black dashed line in Fig. 6).

In order to cross check whether the obtained fitting parameters are reasonable, we have applied them to estimate the concentrations of the related donor impurities. The oscillator strength of the D^0X resonance depends on the donor concentration N as described by²⁷

$$f = \frac{4\pi N}{E_{0,DX}} \left(\frac{\hbar e |P_{cv}|}{m_0 E_{0,DX}} \right)^2 \left[\int \psi(r,0) dr \right]^2, \quad (3)$$

where P_{cv} is the momentum matrix element, e is the electron charge, and m_0 is the free-electron mass. The exciton wavefunction $\psi(r, \rho)$ has the form¹⁴

$$\psi(r, \rho) = \frac{1}{\pi R^{3/2} a_B^{3/2}} \exp(-r/R) \exp(-\rho/a_B). \quad (4)$$

Here ρ denotes the relative electron-hole vector, r is the position of the center of mass, a_B is the Bohr radius ($a_B = 2.34$ nm),²⁸ and R is the localization radius taken equal to a_B . Taking values of P_{cv} from Ref. 29, the total residual donor concentration can be estimated to be about 2×10^{15} cm⁻³ for the Denpa ZnO, which is reasonable for the high-quality material. The value is higher for the Cermet sample, which is consistent with a higher position of the Fermi level such that the donor levels are readily occupied by electrons in dark in this material as revealed from our earlier electron spin-resonance studies.³⁰ A higher concentration of residual impurities could also somewhat explain enhanced light scattering in this material.

The obtained excellent agreement between the experimental data and simulated spectral dependence of polariton-group velocity evidences that the observed decrease of the light velocity in the vicinity of the absorption edge is caused by the formation of exciton-polaritons and is determined by their dispersion. Furthermore the performed simulations allow us to elucidate contributions of different resonances to the slowdown effect. For the $\mathbf{E} \perp \mathbf{c}$ polarization the polariton-group velocity is shown to be mainly determined by the tail of the spectral dispersion within the lower branch of the $FX_A(\Gamma_5)$ polaritons, whereas contributions of the D^0X_A polaritons become important only in close proximity of the corresponding resonances (i.e., within ~ 10 meV for Cermet ZnO). This is obvious from the results of the simulations performed by omitting all D^0X resonances (see the red dotted line in Fig. 6). The minor role of the D^0X_A polaritons could be attributed to the weaker oscillator strength of the D^0X_A excitons as compared with the FX_A transitions for the $\mathbf{E} \perp \mathbf{c}$ polarization. Consistently the dominant effect responsible for the reduction of light velocity for the $\mathbf{E} \parallel \mathbf{c}$ polarization is the $FX_C(\Gamma_1)$ polariton formation.

Based on the obtained parameters for the D^0X_A resonances, we can also briefly discuss to what extent the polariton concept is adequate for the description of BXs in the investigated samples. The polariton framework is usually applied in the case of strong exciton-photon coupling, which is valid when $E_{0,i}^2 f_i / E\Gamma \geq \epsilon_\infty$.¹² This condition is fulfilled for the Cermet ZnO with the higher concentration of residual donors where $E_{0,i}^2 f_i / E\Gamma \sim 20$ (if using the combined oscillator strengths

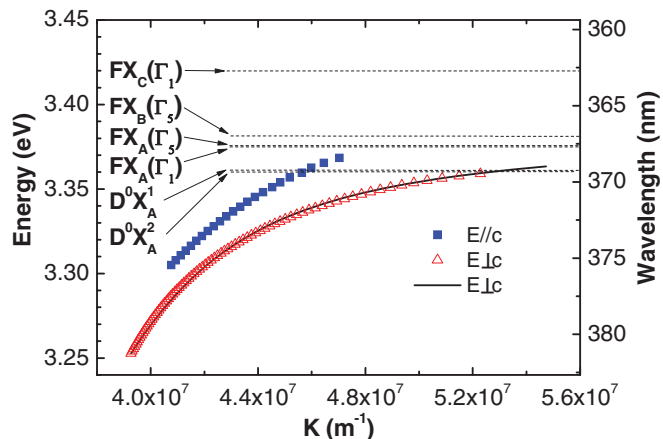


FIG. 7. (Color online) Polariton dispersion within the lower polariton branch, calculated based on the measured group velocity. The results of the calculations for $E \perp c$ and $E \parallel c$ light polarizations are shown by the open triangles and the filled squares, respectively. The horizontal dotted lines denote the spectral positions of the specified excitonic resonance. The open triangles (the solid line) for $E \perp c$ represent the polariton dispersion obtained taking into account (neglecting) data in the vicinity of the D^0X_A resonances.

of D^0X_A). On the other hand light is only weakly coupled to the D^0X_A excitons in the Denpa ZnO. However, even in the latter case the performed analysis using Eq. (2) (including the D^0X_A contributions) is believed to be relevant as the weak-coupling limit is an extreme case of the exciton-photon coupling.^{12,31,32}

C. Polariton dispersion

Based on the experimentally determined spectral dependence of the polariton-group velocity, we can also reconstruct the polariton dispersion within the low polariton branch. Indeed from Eq. (1) the polariton dispersion could be derived as

$$K(E) = K_0(E_0) + \frac{1}{\hbar} \int_{E_0}^E \frac{1}{v_g(E)} dE. \quad (5)$$

Therefore the dispersion in the near-resonance spectral range can be obtained by integrating the experimentally measured $v_g(E)$ dependence (Fig. 6), provided that far from the resonance the polariton energy (E_0) and the corresponding wavevector (K_0) are known. The results of the calculations for $E \perp c$ and $E \parallel c$ light polarizations are shown in Fig. 7. Here we used $E_{0,\perp} = 3.25$ eV, $K_{0,\perp} = 3.92 \times 10^7$ m⁻¹, and $E_{0,\parallel} = 3.30$ eV, $K_{0,\parallel} = 4.07 \times 10^7$ m⁻¹, based on reported values of the refractive index of ZnO.³³ The open triangles (the solid line) for $E \perp c$ represent the polariton dispersion obtained taking into account (neglecting) data in the vicinity of the D^0X_A resonances. The lower polariton branch exhibits a photon-like dispersion in the spectral region transparent to light, which becomes exciton-like when approaching the FX resonances, consistent with the expected dispersion for exciton-polaritons. It is also obvious that the dispersion is mainly determined by the photon coupling with the FXs.

V. CONCLUSIONS

In conclusion, we have employed the time-of-flight spectroscopy to study light propagation through the ZnO media. The group velocity of light is found to dramatically decrease down to 2044 km/s when photon energies approach the absorption edge of the material. It is also demonstrated that the magnitude of this slowdown of light can be controlled by changing light polarization. The effect is explained within the polariton framework and is concluded to be mainly determined by the dispersion of FX polaritons, which propagate coherently via ballistic transport. Based on the experimentally obtained spectral dependence of the polariton-group velocity, the polariton dispersion within the lower polariton branch is accurately determined.

ACKNOWLEDGMENT

Financial support by the Swedish Research Council (Grant No. 621-2010-3971) is greatly appreciated.

*iribu@ifm.liu.se

¹M. D. Lukin and A. Imamoglu, *Nature* **413**, 273 (2001).

²A. V. Turukhin, V. S. Sudarshanam, M. S. Shahriar, J. A. Musser, B. S. Ham, and P. R. Hemmer, *Phys. Rev. Lett.* **88**, 023602 (2002).

³M. Bajcsy, A. S. Zibrov, and M. D. Lukin, *Nature* **426**, 638 (2003).

⁴J. T. Mok and B. J. Eggleton, *Science* **433**, 811 (2005).

⁵C. J. Chang-Hasnain and S. L. Chuang, *J. Lightwave Technol.* **24**, 4642 (2006).

⁶A. Matsko, Y. Rostovtsev, H. Cummins, and M. Scully, *Phys. Rev. Lett.* **84**, 5752 (2000).

⁷Y. A. Vlasov, M. O'Boyle, H. F. Hamann, and S. J. McNab, *Nature* **438**, 65 (2005).

⁸Y. Okawachi, M. S. Bigelow, J. E. Sharping, Z. Zhu, A. Schweinsberg, D. J. Gauthier, R. W. Boyd, and A. L. Gaeta, *Phys. Rev. Lett.* **94**, 153902 (2005).

⁹C. Liu, Z. Dutton, C. H. Behroozi, and L. V. Hau, *Nature* **409**, 490 (2001).

¹⁰D. Phillips, A. Fleischhauer, A. Mair, R. Walsworth, and M. D. Lukin, *Phys. Rev. Lett.* **86**, 783 (2001).

¹¹T. Itoh, P. Lavallard, J. Reydillet, and C. Benoit, *Sol. State Commun.* **37**, 925 (1981).

¹²S. Chu and S. Wong, *Phys. Rev. Lett.* **48**, 738 (1982).

¹³M. Kuwata, T. Kuga, H. Akiyama, T. Hirano, and M. Matsuoka, *Phys. Rev. Lett.* **61**, 1226 (1988).

¹⁴T. V. Shubina, M. M. Glazov, A. A. Toropov, N. A. Gippius, A. Vasson, J. Leymarie, A. Kavokin, A. Usui, J. P. Bergman, G. Pozina, and B. Monemar, *Phys. Rev. Lett.* **100**, 087402 (2008).

¹⁵T. Godde, I. A. Akimov, D. R. Yakovlev, H. Mariette, and M. Bayer, *Phys. Rev. B* **82**, 115332 (2010).

¹⁶K. Ogawa, T. Katsuyama, and H. Nakamura, *Phys. Rev. Lett.* **64**, 796 (1990).

¹⁷J. Lagois, *Phys. Rev. B* **23**, 5511 (1981).

¹⁸G. Blattner, G. Kurtze, G. Schmieder, and C. Klingshirn, *Phys. Rev. B* **25**, 7413 (1994).

- ¹⁹S. F. Chichibu, T. Sota, G. Cantwell, D. B. Eason, and C. W. Litton, *Jap. J. Appl. Phys.* **93**, 756 (2003).
- ²⁰M. Zamfirescu, A. Kavokin, B. Gil, G. Malpuech, and M. Kaliteevski, *Phys. Rev. B* **65**, 161205 (2001).
- ²¹G. Xiong, J. Wilinson, K. B. Ucer, and R. T. Williams, *J. Phys. Condens. Matter* **17**, 7287 (2005).
- ²²D. G. Thomas, *J. Phys. Chem.* **15**, 86 (1960).
- ²³W. R. L. Lambrecht, A. V. Rodina, S. Limpijumnong, B. Segall, and B. K. Meyer, *Phys. Rev. B* **65**, 075207 (2004).
- ²⁴C. Klingshirn, *Phys. Stat. Sol. (b)* **244**, 3027 (2007).
- ²⁵M. Cobet, C. Cobet, M. R. Wagner, N. Esser, C. Thomsen, and A. Hoffmann, *Appl. Phys. Lett.* **96**, 031904 (2010).
- ²⁶B. K. Meyer, H. Alves, D. M. Hofmann, W. Kriegseis, D. Forster, F. Bertram, J. Christen, A. Hoffmann, M. Straßburg, M. Dworzak, U. Haboeck, and A. V. Rodina, *Phys. Stat. Sol. (b)* **241**, 231 (2004).
- ²⁷E. L. Ivchenko, *Optical Spectroscopy of Semiconductor Nanostructures* (Alpha Science, Harrow, UK, 2005), p. 627.
- ²⁸Y. Gu, I. L. Kuskovsky, M. Yin, S. O'Brien, and G. F. Neumark, *Appl. Phys. Lett.* **85**, 3833 (2004).
- ²⁹S. Shokhovets, O. Ambacher, B. K. Meyer, and G. Gobsch, *Phys. Rev. B* **78**, 035207 (2008).
- ³⁰X. J. Wang, L. S. Vlasenko, S. J. Pearton, W. M. Chen, and I. A. Buyanova, *J. Phys. D: Appl. Phys.* **42**, 175411 (2009).
- ³¹P.Y. Yu and M. Cardona, *Fundamentals of Semiconductors* (Springer-Verlag, Berlin, 1999), p. 620.
- ³²C. Klingshirn, *Semiconductor Optics* (Springer-Verlag, Berlin, 2005), p. 797.
- ³³Y. S. Park and J. R. Schneider, *J. Appl. Phys.* **39**, 3049 (1968).